EXPERIMENTAL INVESTIGATIONS OF AN ICING PROTECTION SYSTEM FOR UAVS

Richard Hann[1], Kasper Borup[1], Artur Zolich[1], Kim Sorensen[2], Håvard Vestad[1], Martin Steinert[1], and Tor Arne Johansen[1]
[1]Norwegian University of Science and Technology (NTNU)
[2]UBIQ Aerospace

Abstract

UAV icing is a severe challenge that has only recently shifted into the focus of research. Today, there are no mature icing mitigation technologies for UAVs, except for the largest fixed-wing drones. We are working on the development of an electro-thermal icing protection technology called D•ICE for medium-sized fixed-wing UAVs. As part of the design process, an experimental test campaign at the Cranfield icing wind tunnel has been conducted. This paper describes the icing protection system and shares experimental results on its capability for icing detection and anti-icing. Icing detection is based on an algorithm evaluating temperature signals that are induced on the leading-edge of the wing. A baseline signal is generated during dry (icing cloud off) conditions and compared to a signal during wet (icing cloud on) conditions. Due to significant differences in the heat transfer regime, the system can differentiate between these two states. The experiments show that our system can reliably detect icing conditions based on this principle. Furthermore, the anti-icing capability of the system is proven for two icing cases. The minimal required heat flux to keep the surface ice-free was obtained by gradually reducing power supply to the heating zones until icing could be detected. These experimental results were compared to FENSAP-ICE simulations. The test campaign includes a successful fully-autonomous run, where the system automatically detected icing and initiated suitable anti-icing measures.

Introduction

Atmospheric icing imposes a significant limitation on the operational envelope of unmanned aerial vehicles (UAVs) [1]. While there is a good understanding of icing for general aviation [2], few studies focus on UAV icing. The existing studies indicate that icing on a UAV degrades the aerodynamic performance by reducing lift, increasing drag and negatively affecting the stall behavior [3–7]. All these factors constrain the flight envelope and significantly increase the risk of losing the aircraft. In order to mitigate the adverse effects of icing, suitable icing protection systems (IPS) are required. For commercial and military aviation a wide range of mature icing protection systems exist [8], whereas such solutions are very limited for medium-sized UAVs.

Fixed-wing UAVs with wing-spans of several meters are suited for many autonomous applications. For example, such UAVs can be used for remote sensing, search and rescue, oil spill detection, ship-based iceberg tracking, transportation of goods [9]. Typical mission profiles require the capability to operate autonomously, beyond line of sight, for extended periods, in all weather conditions. The adverse effects of in-cloud icing prevent UAV to execute these aforementioned tasks. Essentially, UAVs today are grounded during icing conditions or face a substantial risk of crashing [10]. Therefore, developing a suitable IPS for UAVs is one of the key challenges for the use of small to medium sized autonomous fixed-wing UAVs in the future.

A multitude of technical IPS solutions exist for manned aviation [8], but are only partly transferable to UAVs. There are several key differences between manned and unmanned aircraft. UAVs are typically smaller in size. This implies that there are more strict weight and dimensional constraints to an IPS. Consequently, power is a limited resource on UAVs which means that the IPS needs to be particularly energy efficient. The only available energy form is usually electric. Icing detection on a UAV needs to be fully autonomous [11], which is similar to wind turbine icing [12]. The instrumentation for detection should be minimal and energy efficient. Last but not least, UAVs are less cost-intensive compared to manned aircraft, which means that smaller budgets are available for IPS developments. This creates an opportunity for extensively using numerical simulation methods to support and guide the IPS design process. However, the available icing simulation tools have been developed for aircraft applications and are not validated for the Reynolds number regime of UAVs, which is a current limitation [13].

Researchers at the Research Centre of Excellence the Autonomous Marine Operations and Systems (AMOS) under the Norwegian University of Science and Technology (NTNU), have developed the IPS technology called D•ICE. D•ICE is a modular, robust, power-efficient, and autonomous icing protection solution that encompasses icing detection and removal capabilities. It enables continuous unmanned aircraft operations globally and in the harshest conditions [11]. D•ICE is based on an electro-thermal heating system, and novel estimation, control, and detection algorithms. The technology has been through a comprehensive proof-of-concept study and is being commercialized by UBIQ Aerospace. Since the beginning of that project in 2013, the system has been integrated into several different types and sizes of fixed-wing unmanned aircraft and been tested in icing wind tunnels and in flight. This study describes an experimental test campaign that has been conducted at the Cranfield icing wind tunnel on that system during autumn 2018. The system has been tested with regards to its capabilities for icing detection, anti-icing, and fully autonomous operation.

Figure 1. Icing protection system with five heating zones inside the wind tunnel. Four additional thermocouples have been added (blue tape).

Method

The Cranfield icing wind tunnel is a closed-loop tunnel with a cooling capacity of 450kW and a test section of 760x760mm [14]. The studied airfoil is a RG-15 with a thickness of 8.9% and a chord of 450mm, spanning the entire width of the test section The RG-15 is a low-Reynolds airfoil used for a wide range of UAV and model aircraft applications.

Multiple prototype probes of the airfoil, based on wayfaring principles [15], were made to determine the fastest and most cost-efficient way to produce the model. The final wing-design was constructed from layered, laser-cut ribs of medium-density fiberboard (MDF), which was then covered with 1mm high impact polystyrene (HIPS) sheet. Through testing, the material was determined to be able to withstand the chemicals in the nanocarbon heating paint. The foil coating allowed for a smooth surface with little need for extensive surface finishing. The HIPS foil along the leading-edge was heat bent to reduce stress and potential fracture, while the trailing edge was constructed of solid layered MDF to enable a large gluing area.

A total of five heating zones were applied to the wing using a carbon nanotube paint that functions as an electro-thermal heating source, see Fig. 1. Each heating zone was 5.4cm wide and covered the entire span of the wing. The paint is using an acrylate bonding system with nanocarbon additives. This results in conductive paint coatings that generate heat when passed through by electric current. Power was supplied and monitored for each zone individually. In the scope of this study, only the leading-edge zone was used. Power delivery to the heating was regulated by using pulse-width modulation (PWM) [16]. Each zone was equipped with a cement on polyimide T-type thermocouple, located underneath the coating, as well as additional external thermocouples (applied with blue tape, see Fig. 1).

Meteorological conditions were chosen based on typical cruise speeds of fixed-wing UAVs for long-endurance missions. Icing processes are typically described by the velocity v, the temperature T, the liquid water content LWC, the median droplet volume MVD, and the airfoil angle of attack (AOA) α. An overview of the test cases is given in Table 1.

An icing detection concept was tested, that actively uses heat sources to generate a temperature signal. This signal will be characteristic for dry (cloud off, no droplets in the flow), wet (cloud on, droplets in the flow), and iced (ice on airfoil) conditions [11]. The signal was created by heating the leading-edge heating zone for a duration of 10s with a small (~60W) heat spike. Thermocouples were then measuring the resulting temperature changes on the surface for 60s. To distinguish the different environmental conditions, a reference signal was generated for dry conditions. This dry signal was used as a baseline, to which all new signals were compared against. During activation of the icing detection system, temperature signals were generated every 70s and compared to the baseline signal. The root-mean-square error (RMSE) between the observed and reference signal was then calculated. The value of the RMSE serves as an indicator for identifying different environmental conditions. In order to test the functionality of the system, a series of tests at different conditions was conducted. The tests aimed to answer the following question:

Table 1. Meteorological and flight conditions for the ice detection, anti-icing and full system runs

run	Cloud	T [°]	MVD [µm]	LWC [g/m³]	v [m/s]	AOA [°]	RMSE	RMSE (scaled)
#1	Dry	-5	-	-	25	0	0.10	0.07
#2	Wet	-5	20	0.56	25	0	1.21	0.55
#3	Wet	-10	20	0.72	25	0	2.00	0.62
#4	Iced	-10	20	0.72	25	0	1.80	0.31
#5	Dry	-10	-	-	25	4	0.83	0.13
#6	Wet	-10	20	0.72	25	4	1.74	0.71
#7	Wet	+5	20	0.56	25	0	1.43	0.12
#8	Wet	-5	20	0.56	25	0	Anti-Icing	
#9	Wet	-5	20	0.56	25	0	Anti-Icing	
#10	Wet	-10	20	0.72	25	0	Anti-Icing	
#11	Variable	-5	20	0.56	25	0	Full System Test	

- Can different icing conditions be identified by the detection method?
- Is the system able to detect if ice has already built up on the surface?
- Does the detection algorithm give false alerts if the ambient temperature or the angle of attack changes from the baseline?
- How does the system behave when it encounters a non-freezing cloud?

Answering these questions allows setting an RMSE threshold value that can identify icing conditions. Once hazardous conditions are identified, the heating zones are activated for anti-icing operations. Continuous heating of the leading-edge will prevent ice from accumulating on the surface and therefore mitigates the adverse effects of icing. The system was designed as running-wet, i.e. the incoming droplets are prevented from freezing but not fully evaporated. This introduces the risk of runback icing, which was observed but not studied in detail during this study.

A key question for the operation of an anti-icing system is the required surface heat fluxes to prevent ice formation. To achieve this, the surface temperature always must be kept above the freezing temperature. The minimum heat flux requirement of the anti-icing system needs to compensate for all heat losses that occur during icing [17]. This includes convective heat losses, evaporation, impinging heat of the droplets, and radiation.

As part of this study, the minimum required heat fluxes for anti-icing have been determined experimentally. This was achieved by operating the anti-icing system with high initial power (6–8kW/m²), which was then step-wise decreased until ice accretion was observed on the leading-edge of the airfoil. Each step the power was decreased by approximately 10%. The power was held for 90s during which time the surface was monitored for ice accretion through a 250mm

camera lens. If no ice was detected, the power was decreased. This was repeated until ice accretion was observed. The power setting for the last step where no icing occurred, was then defined as the minimum required anti-icing heat flux. This method has been performed twice at identical icing conditions to test the repeatability of the results, and once at a lower temperature. These experimental values are then compared to FENSAP-ICE simulation results.

Last but not least, a full system test was conducted, where the anti-icing system was automatically activated once a pre-set RMSE threshold was exceeded. The algorithm for the full system test cycles through the following three modes: step, cool, detect. The 'step' command lasts 10 seconds and for those 10 seconds, the leading-edge zone is heated with a low PWM value. The 'cool' phase lasts 60 seconds – about the amount of time needed until the temperature of the zone has returned to the pre-heat value. The 'detect' command evaluates the temperature signal measured during 'step' and 'cool' to infer whether ice accretion occurs on the airfoil. The detection algorithm uses the captured temperature signal and compares this to a reference signal captured under dry conditions. The RMSE between the two signals is then compared to a threshold value chosen based on previous data. This cycle of three sequential commands continues to run until the system detects ice accretion. When ice is detected, the system switches into an anti-icing mode, where the PWM value of the zone is set to a pre-defined value, that is high enough to prevent ice from building up on the leading-edge.

The experiments will be accompanied by numerical simulations. The icing code ANSYS FENSAP-ICE (v19.2) is used to estimate the minimum required heat fluxes for running-wet anti-icing. FENSAP-ICE is a state-of-the-art computational fluid dynamics (CFD) icing code that is able to simulate ice accretion, performance degradation and anti-icings loads [18]. FENSAP-ICE has been used to estimate anti-icing loads on UAVs before [13], however, due to a lack of experimental data on UAV IPS, the tool is not validated. The FENSAP-ICE simulations are based on monodisperse droplet distributions, calculated on a hybrid 2D mesh with no heat conduction into the airfoil. The predicted heat fluxes are obtained by solving the thermodynamical equations on the surface to maintain a surface temperature of zero degree [19].

Icing Detection

The first set of experiments were aimed to calibrate and test the icing detection method during different conditions, which are presented in Table 1. following conditions were considered:

- No icing cloud / dry conditions: runs #1, #5.
- Freezing icing cloud / wet conditions: runs #2, #3, #6.
- Non-freezing cloud / wet conditions: run #7.
- Ice present on airfoil but no cloud / iced conditions: run #4.

The reference signal was obtained during a dry run with an ambient temperature of T=−5°C. Figure 2 compares the reference signal to a detection signal at identical conditions. This results – as expected – with a very low RMSE and serves as proof that the detection algorithm is able to identify non-icing conditions when the temperature and the flow field are unchanged.

Figure 3 shows the "wet, freezing" conditions for a detection signal taken immediately after the droplet cloud was turned on, at the same temperature as the reference signal. It is obvious that the signal during icing conditions is significantly dissimilar to the reference signal, in shape and maximum temperature change. The RMSE for this initial case was 1.06 which increased to 1.21 during the following detection cycle. This indicates that there is a time dependency on the RMSE signal. The difference between the reference signal and the detection signal under icing conditions will increase with time. This mechanism seems to work fairly quickly and is most likely related to the release of latent heat during freezing in combination with the increased roughness and heat transfer on the surface.

A second test under icing condition was performed, however, at lower temperatures, see Fig. 4. The difference between the detection signal and the reference signal for this case was even more pronounced and results with an initial RMSE value of 2.00. This test was then continued for a total icing duration of 5min, after which a thin continuous ice layer of approximately 2–3mm formed on the leading edge. After this, the droplet cloud was turned off in order to investigate how the detection system would react to the presence of ice on the surface. The resulting detection signal is shown in Fig. 5. The lack of droplet impingement leads to higher temperatures of the detection signal and leads to an overall reduced RMSE of 1.80. These results show that the sensitivity of the detection system seems to depend on the icing temperature. Larger temperature differences seem to increase the RMSE and increase the detectability of icing conditions. This should be considered in the future for choosing the conditions of the baseline reference signal. Once ice has formed on the surface, it can still be detected, even if there is no droplet impingement (i.e. the icing cloud has been left) present.

To test the robustness of the system towards false icing alerts, a dry test with an increased angle of attack and reduced air temperature was conducted, see Fig. 6. The detection signal is resulting in a lower temperature increase, which can be attributed to the lower temperatures of the air and airfoil model, as well as to the increased flow velocities near the leading-edge. These differences manifest themselves in an increased RMSE of 0.83 which may be mistakenly interpreted as icing conditions. In order to adjust for the effect of temperature and angle of attack, a constant scaling factor is introduced. This scaling factor scales the temperature signal (in y-direction) optimally in such a way to minimize the RMSE. The resulting, adjusted detection signal is shown in Fig. 7 and reduces the RMSE to 0.13. The same approach is then applied to the same case, but with activated droplet cloud. Figure 8 depicts the initial, unscaled, wet detection signal. This results in an RMSE of 1.74 which is in line with the previous results. With the constant scaling factor, the wet RMSE is reduced to 0.71, see Fig. 9. This approach has been applied to all the other tests as well, with the results shown in Table 1.

The last experimental test was conducted to see how the system reacts to the occurrence of wet conditions with a temperature above freezing. This case occurs when a UAVs is situated within a non-freezing cloud. The signal is shown in Fig. 10 and displays a RMSE of 1.43 which indicates a substantial difference to the dry reference signal. The scaled RMSE of this case was 0.12 which is substantially lower than the absolute value.

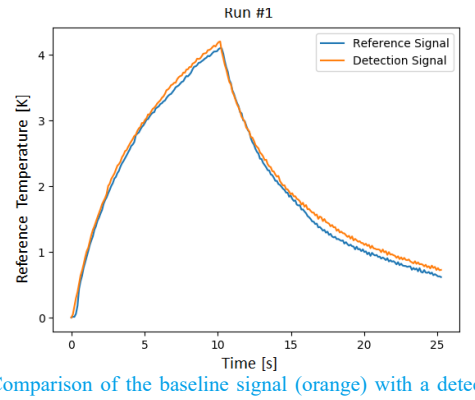

Figure 2. Comparison of the baseline signal (orange) with a detection signal (blue) for dry conditions at T=−5°C.

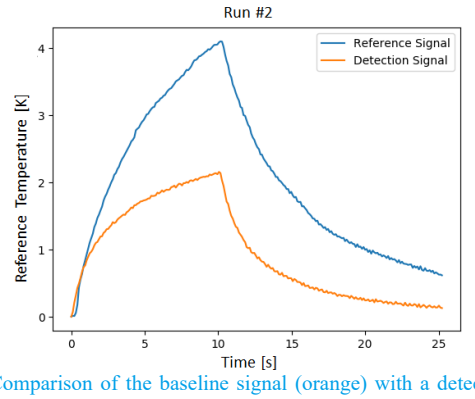

Figure 3. Comparison of the baseline signal (orange) with a detection signal (blue) for wet conditions at T=−5°C.

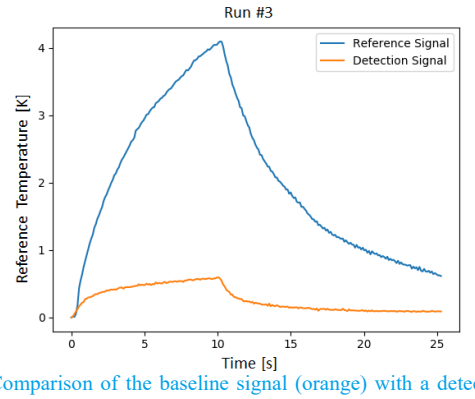

Figure 4. Comparison of the baseline signal (orange) with a detection signal (blue) for wet conditions at T=−10°C.

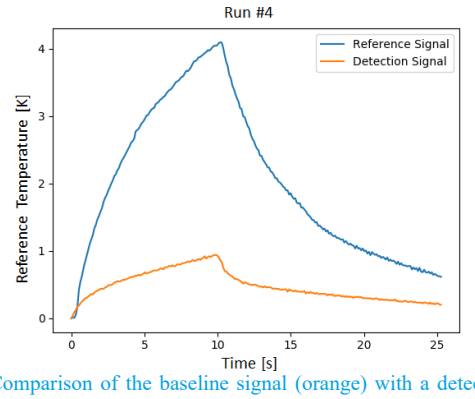

Figure 5. Comparison of the baseline signal (orange) with a detection signal (blue) for iced conditions at T=−10°C.

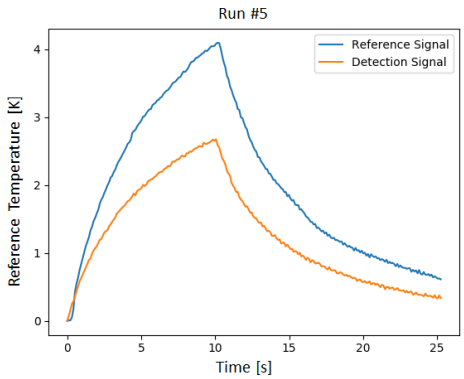

Figure 6. Comparison of the baseline signal (orange) with a detection signal (blue) for dry conditions at T=−10°C and AOA=4°.

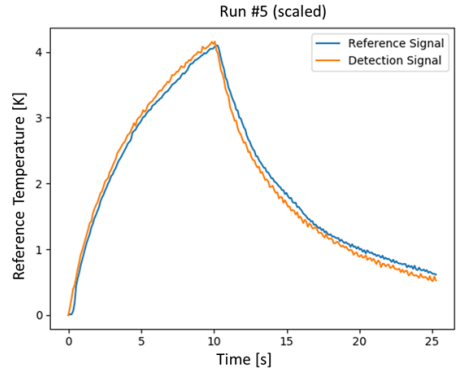

Figure 7. Comparison of the baseline signal (orange) with a scaled detection signal (blue) for dry conditions at T=−10°C and AOA=4°.

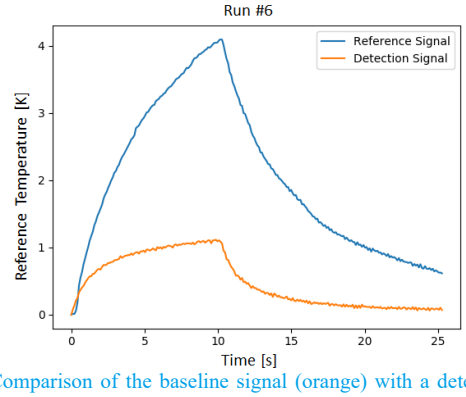

Figure 8. Comparison of the baseline signal (orange) with a detection signal (blue) for wet conditions at T=−10°C and AOA=4°.

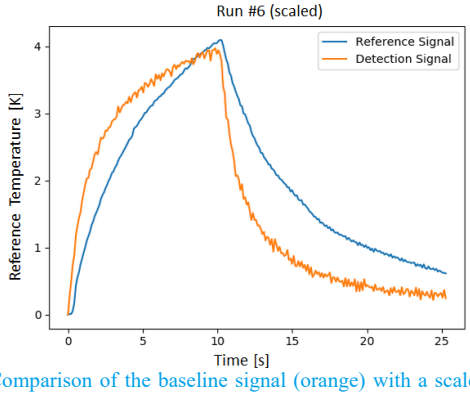

Figure 9. Comparison of the baseline signal (orange) with a scaled detection signal (blue) for wet conditions at T=−10°C and AOA=4°.

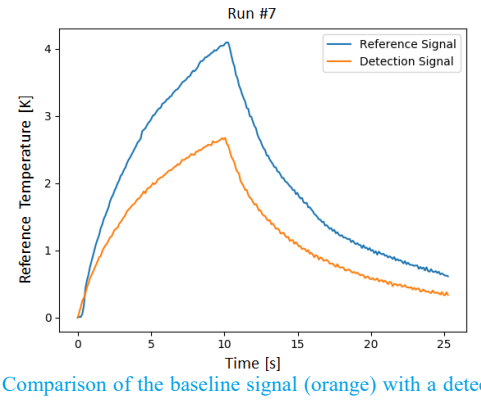

Figure 10. Comparison of the baseline signal (orange) with a detection signal (blue) for wet conditions at T=+5°C.

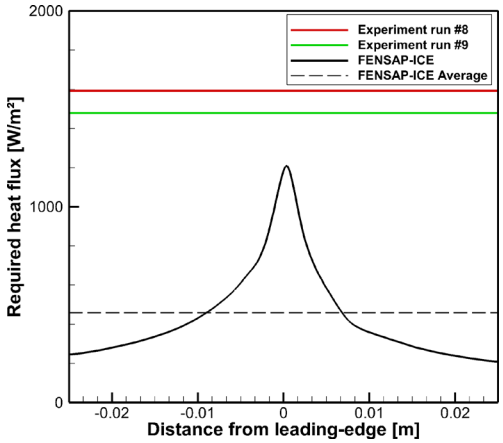

Figure 11. Comparison of the required heat fluxes for anti-icing from the experiments and the numerical simulations with FENSAP-ICE for runs #8–9.

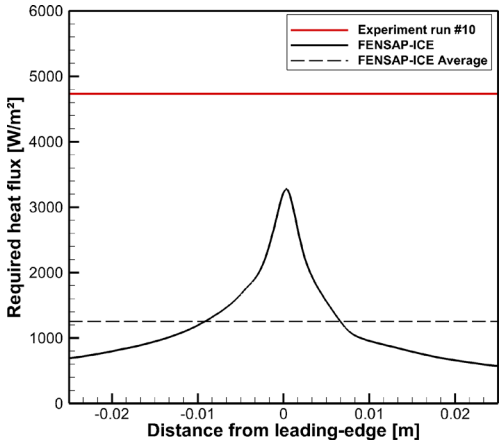

Figure 12. Comparison of the required heat fluxes for anti-icing from the experiments and the numerical simulations with FENSAP-ICE for run #10

Required Anti-Icing Loads

Three experiments to determine anti-icing loads have been performed with the conditions specified in Table 1 (runs #8–10). In addition to the experimental results, FENSAP-ICE simulations have been conducted to simulate the minimum required heat fluxes for anti-icing. The results are presented in Fig. 11 and 12. FENSAP-ICE is predicting a distribution of the heat fluxes over the entire width (indicated by the distance *s* from the leading-edge) of the heating zone, whereas the experiments only yield an averaged value. The simulation results show that the maximum power requirement occur near the leading-edge at the stagnation point. This is the location with the highest droplet impingement rates and thus the highest required heat fluxes. Power requirements diminish quickly as a function of distance from the stagnation point. The average heat requirements from FENSAP-ICE have been calculated by integrating the area under the curves.

The experimental results from the two identical runs indicate that the method is repeatable and the results consistent. Compared to the numerical results, the experimental data indicates about 220–270% higher average heat loads. A possible explanation for this is that the experimentally determined minimal heat flux was mainly driven by the peak anti-icing loads. In fact, the heat flux maximums from FENSAP-ICE are in better match with the experimental data (22–44%). Since the heating zones are located on the outside of the airfoil models, very little heat conduction is occurring inside the material. This means that the average heat flux values may not be a good indicator for the total required heat loads, but that the peak values near the leading-edge are more important.

Full System Test

A full system test of D•ICE, including automatic icing detection and activation of the anti-icing system, was performed to prove the functionality of the system (run #11). Figure 13 shows the details of the case over the runtime. The icing detection algorithm was activated while the cloud was turned off in the wind tunnel. After 180s, the spray bars in the tunnel were turned on. The system was able to identify icing conditions during the second detection cycle, i.e. 140s after the cloud was activated. This activated automatically the anti-icing system which operated at a constant PWM for a total length of 5min during which no significant ice accretion could be observed on the heated zones, see Fig. 14. Note that the picture shows some ice accretion near the window and on the external thermocouples. This is related to the inhomogeneity of the heat distribution near the power connectors on the side of the airfoil, and limited heat conduction on the external thermocouples.

Figure 13 shows that the surface temperature increased rapidly after the anti-icing was turned on and then decreased over the rest of the run duration. This can be most likely explained with the materials positive temperature dependency on the electrical resistance. The current I is inversely proportional to the resistance R and directly proportional to the heat output ($P=U\cdot I^2$). The figure shows that the current goes from being saturated to slowly dropping. The reason why the current is saturated during detection is related to the operational mode of the power supply. As long as the PWM is not set to zero, the full current is provided to the transistors.

Discussion

The presented method for icing detection has been tested for different flight conditions and with two evaluation approaches (RMSE & scaled RMSE). The results in Table 1 show that the temperature response signal shows significant differences between cases with no icing conditions and iced/wet cases. The arising challenge is to determine a threshold value to distinguish the cases from each other.

Figure 15 displays the RMSE and scaled RMSE values for all seven detection cases. Ideally, the threshold value should be selected in a way that it differentiates between the non-icing (runs #1, #5, #7) and the icing cases (runs #2, #3, #4, #6). Using the unscaled RMSE value, this feature cannot be fully achieved, since the RMSE for run #2

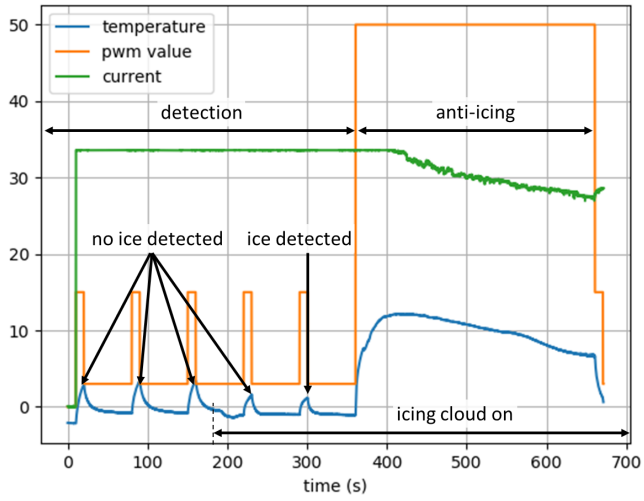

Figure 13. Measurements of temperature, power setting (PWM) and current supplied to the leading-edge heat zone for the full system test, run #11.

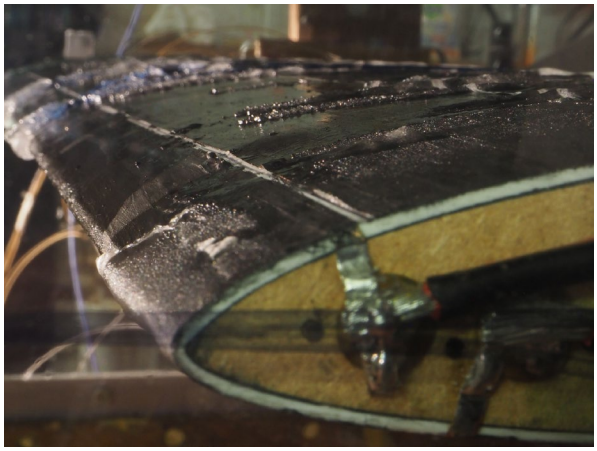

Figure 14. Anti-icing test. Partial ice accretion can be seen near the window and on the external thermocouples due to insufficient heating.

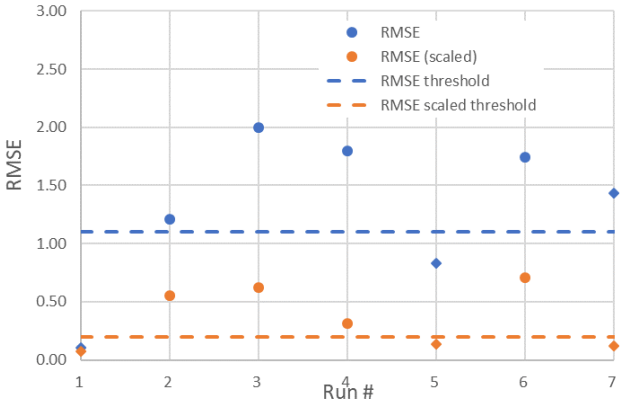

Figure 15. Scaled and unscaled RMSE results for all detection runs with threshold levels to distinguish between non-icing and icing conditions. Iced cases are shown with round symbols and non-iced cases with diamonds

(wet, freezing) is lower than for #7 (wet, non-freezing). However, a threshold can be found that is only discriminating between dry and wet conditions, with a value of 1.10. However, by using the scaled RMSE approach, the differences between the cases become much more pronounced and distinguishable. Therefore, a scaled RMSE threshold value of about 0.20 is suitable to differentiate between the non-icing and icing cases.

These results show the capability of the icing detection method to accurately identify conditions that require the activation of an IPS. The scaled RMSE approach seems better suited than using only the absolute RMSE values. The current scaling approach is very simple and leaves room for implementing more sophisticated comparison methods. Further testing is required to build more confidence in the detection system and to identify appropriate scaling methods. Such tests may be conducted using FENSAP-ICE simulations (e.g. to cover a large range of flight and meteorological conditions) additional icing wind tunnel tests, as well as real-world test flights. Detection cases that have not been investigated yet include freezing rain, freezing drizzle, and ice clouds.

The anti-icing experiments show a reasonably good match with the FENSAP-ICE simulation data if only the maximum heat loads are regarded. Several experimental uncertainties have to be considered for that case. First of all, the heat distribution has not been perfectly homogenous in the leading-edge IPS zone. In particular, the heating has been significantly reduced at the edges of the airfoil, as can be seen in Figure 14. This introduces uncertainty on the surface heat fluxes during the anti-icing experiments. At this stage, this error could not be quantified but was estimated to about 10%. A second error is related to the stepwise power decrease. It was difficult to observe the exact time point when icing started to occur which may have resulted in overly conservative heat flux estimates in the experiment. For future experiments, it is recommended that more time and smaller power-steps are selected in order to improve the experimental data. Also, narrower heating zones would allow to more accurately capture the exact minimum heating values, especially near the leading-edge.

Summary/Conclusions

This study investigated three main challenges that are associated with the development of an IPS for UAVs: icing detection, icing mitigation, and autonomous system operation. An icing detection method which utilizes the surface heating coatings to generate thermal signals was tested for different icing and non-icing conditions. The method compares thermal signals to a reference signal and evaluates the difference to the baseline. The experiments have shown that this approach, when combined with a simple scaling method, can accurately distinguish between icing and non-icing cases.

Icing mitigations were performed with an anti-icing system. In the scope of these experiments, the minimum required heat flux to keep the surface free of ice was determined for two meteorological conditions by stepwise reduction of the power supplied to the system. The results were compared to numerical simulations in FENSAP-ICE for validation purposes. The experiments indicated that the peak power requirements near the leading-edge drive the minimum heat fluxes in the experiment. The values compare well with the numerical method. However, the results were not accurate enough to fully validate the numerical methods and more detailed work will be required for higher confidence.

A full system test was conducted, which automatically detected the onset of icing conditions and autonomously initiated mitigation measures in the form of anti-icing. The test proved that the D•ICE technology has the capabilities to successfully protect a lifting surface from the adverse effects of icing.

References

1. Siquig, A., “Impact of Icing on Unmanned Aerial Vehicle (UAV) Operations,” Naval Environmental Prediction Research Facility, 1990, doi:test123.

2. Bragg, M.B., Broeren, A.P., and Blumenthal, L.A., “Iced-airfoil aerodynamics,” *Prog. Aerosp. Sci.* 41(5):323–362, 2005, doi:10.1016/j.paerosci.2005.07.001.

3. Tran, P., Baruzzi, G., Tremblay, F., Benquet, P., Habashi, W.G., Petersen, P.B., Liggett, M.W., and Fiorucci, S., “FENSAP-ICE applications to unmanned aerial vehicles (UAV),” *42nd AIAA Aerospace Sciences Meeting and Exhibit*, 390–402, 2004.

4. Szilder, K. and Yuan, W., “In-flight icing on unmanned aerial vehicle and its aerodynamic penalties,” *Prog. Flight Phys.* 9:173–188, 2017, doi:10.1051/eucass/201709173.

5. Williams, N., Benmeddour, A., Brian, G., and Ol, M., “The effect of icing on small unmanned aircraft low Reynolds number airfoils,” *17th Australian International Aerospace Congress*, AIAC, Melbourne, 2017.

6. Hann, R., Wenz, A., Gryte, K., and Johansen, T.A., “Impact of atmospheric icing on UAV aerodynamic performance,” *2017 Workshop on Research, Education and Development of Unmanned Aerial Systems, RED-UAS 2017*, Linköping, ISBN 9781538609392: 66–71, 2017, doi:10.1109/RED-UAS.2017.8101645.

7. Hann, R., “UAV Icing: Comparison of LEWICE and FENSAP-ICE for Ice Accretion and Performance Degradation,” *2018 Atmospheric and Space Environments Conference*, AIAA Aviation, Atlanta, ISBN 978-1-62410-558-6, 2018, doi:10.2514/6.2018-2861.

8. Goraj, Z., “An Overview of the Deicing and Antiicing Technologies with Prospects for the Future,” *24Th Int. Congr. Aeronaut. Sci.* 1–11, 2004.

9. Hann, R., “Opportunities and Challenges for Unmanned Aerial Vehicles (UAVs) in the Arctic,” *13th ArcticNet Annual Scientific Meeting*, 2017.

10. Peck, L., Ryerson, C.C., and Martel, C.J., “Army Aircraft Icing Cold Regions Research and Engineering Laboratory,” Cold Regions Research and Engineering Laboratory, 2002.

11. Sørensen, K.L., “Autonomous Icing Protection Solution for Small Unmanned Aircraft,” NTNU, ISBN 987-82-326-1889-7, 2016.

12. Battisti, L., “Wind Turbines in Cold Climates,” Springer, 2015.

13. Hann, R., “UAV Icing: Comparison of LEWICE and FENSAP-ICE for Anti-Icing Loads,” *AIAA Scitech 2019 Forum*, AIAA, San Diego, ISBN AIAA 2019-1286, 2019, doi:10.2514/6.2019-1286.

14. Hammond, D.W. and Luxford, G., “The Cranfield University Icing Tunnel,” *41st Aerospace Sciences Meeting and Exhibit*, 2003.

15. Steinert, M. and Leifer, L.J., “Finding One’s Way: Re-Discovering a Hunter-Gatherer Model based on Wayfaring,” *Int. J. Eng. Educ.* 28(2), 2012.

16. Holmes, D.G. and Lipo, T.A., “Pulse width modulation for power converters: principles and practice,” John Wiley & Sons, 2003.

17. Dillingh, J.E. and Hoeijmakers, H.W., “Numerical simulation of airfoil ice accretion and thermal anti-icing systems,” *ICAS Congress Proceedings*, 2004.

18. Habashi, W.G., “Recent Progress In Unifying CFD and In-Flight Icing Simulation,” 2010.

19. Héloïse, B., François, M., and Wagdi G., H., “FENSAP-ICE’s three-dimensional in-flight ice accretion module: ICE3D,” *J. Aircr.* 40(2), 2003.

Contact Information

Richard Hann, richard.hann@ntnu.no
O.S. Bragstads plass 2D, NO7491 Trondheim, Norway

Acknowledgments

This project has received funding from the Research Council of Norway under grant number 237906, Centre for Integrated Remote Sensing and Forecasting for Arctic Operations (CIRFA). The research was also funded by grant number 223254, Centre for autonomous marine operations and systems (NTNU AMOS). Further funding was received from the Norwegian Research Council FORNY, grant number 284649, and the Regionalt Forskningsfond Midt-Norge, grant number 285248. Special thanks to Hugo Pervier and Peter West from Cranfield University, who were an integral part of this work and were very helpful at all times.